

Investigations on entrainment of surrounding fluid in jet flow in to a cylindrical tube nozzle

Pramod Kuntikana*
Indian Institute of Technology,
Bombay, India
pramodkuntikana@gmail.com

Ravikiran Kadoli
National Institute of Technology
Karnataka, Surathkal, India
rkkadoli@nitk.ac.in

S. V. Prabhu
Indian Institute of Technology,
Bombay, India
svprabhu@iitb.ac.in

ABSTRACT

Jet flow is employed in numerous cooling and heating applications because of its higher heat transfer coefficient. The entrainment of secondary fluid plays an important role in certain applications such as mixing tube of self aspirating burners and injector of pulse jet filter bags. Designs including proper utilization of secondary entrained fluids will reduce the energy consumption in mixing and compression of the fluid. The entrainment is to be minimised for the applications including jet cooling or heating where the surrounding fluid will thermally dilute the flow. The present study experimentally investigates the effect of various parameters such as jet Reynolds number, orifice to tube spacing, and orifice diameter on jet entrainment for a cylindrical tube nozzle. The maximum entrainment coefficient is obtained at the axial location where the tube diameter is comparable with the jet width. Overall entrainment coefficient of 0.318 is obtained.

KEY WORDS

jet entrainment, Reynolds number, tube nozzle, pressure

1.0 INTRODUCTION

Jet flow finds numerous applications in cooling and heating appliances. Synthetic jet cooling for electronic components [1], jet impingement cooling of gas turbine blades [2, 3], mixing tube of the burners [4, 5, 6, 7], nozzles in jet pump [8], nozzle of pulse jet bag filters [9, 10, 11] etc. are some of the engineering applications of the jet flow. The jet flow entrains the surrounding fluid to the main stream due to the pressure gradient between the jet flow and the ambient. The

secondary entrained fluid brings down the momentum of the primary jet flow along the jet axis [12]. The entrainment enhances the mixing between the primary fluid and the secondary entrained flow. The jet fluid gets thermally diluted if there is a temperature difference between the surrounding and the jet fluids. This occurrence is known as thermal entrainment. The entrainment phenomenon helps in self aspirating burners to mix the fuel and air to have a homogeneous mixture at the burner ports [13]. However, after the combustion at the burner ports, flame jet dilution is caused by the entrainment of the ambient air with the hot combustion gas. This adversely affects thermal performance of the burners. The pressure gradient caused by the jet flow is used to suck the secondary fluid and pump it to desired height in jet pumps. The pulse jet filter bags utilise a pulse jet to clean the dust cake formed on the surface of the filter bag [11]. The entrainment helps here to reduce energy consumption. Yadav et al. [14] studied the mixing and entrainment characteristics of pulsating jets. MacGregor [15] performed experimental investigations on entrainment in spray jets. The entrainment phenomenon is governed by the jet velocity, the density, temperature of the jet and surrounding fluid, nozzle diameter and axial distance. The present study attempts to investigate the influence of various parameters on the secondary fluid entrainment in jet flow. An experimental facility is fabricated in-house to measure the secondary fluid entrainment in jet flow. Experiments are conducted with air for various nozzle diameters, jet Reynolds numbers and axial distances. The entrainment coefficient is determined for various jet configurations. Table 1 shows the matrix of experimental

parameters.

Table 1-Matrix of experimental parameters

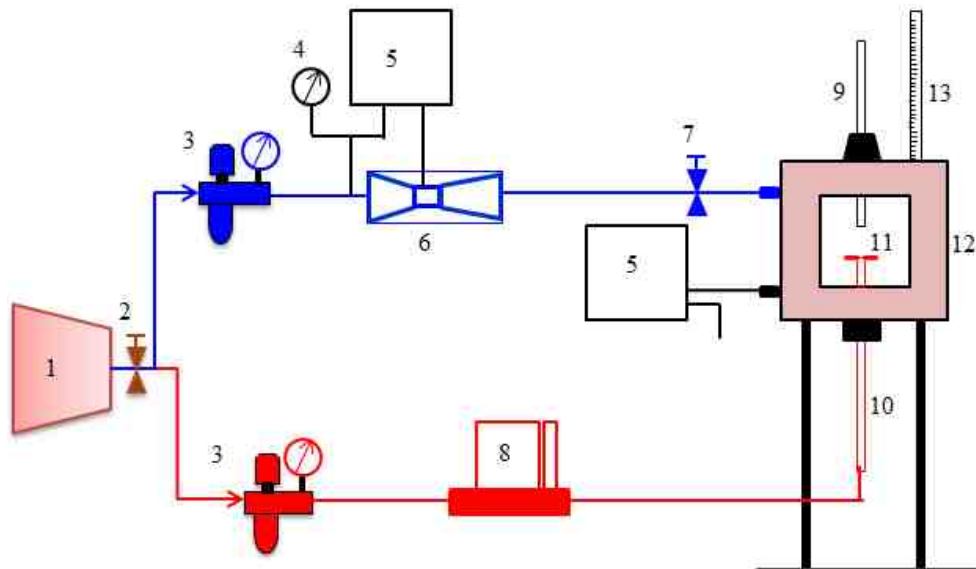
<i>Re</i>	<i>d/D</i>	<i>Z/d</i>
4000, 6000,	0.05, 0.1,	0, 1, 2, 3, 4, 5, 6,
8000, 10000,	0.15, 0.2	7, 8, 9, 10, 15, 20,
12000 and	and 0.25	30, 40, 50, 60, 70,
15000		80, 90 and 100

2.0 EXPERIMENTAL SET UP

Figures 1 and 2 respectively show the schematic and photograph of the experimental set up used in the present study. The compressed air is supplied from receiver tank of the screw compressor through a needle valve. Two separate flow lines are used for primary jet fluid and secondary fluid which is entrained. The line pressures of both lines are regulated with independent pressure regulators. The air filters are inserted along with the pressure regulators to filter the external particles and oil residues. The primary flow is metered through Aalborg (USA) make mass flow controller (MFC). The MFC has flow range of 0 to 66 SLPM, is calibrated with BIOS make DryCal Defender 30H gas flow calibrator with an accuracy of 1% reading attributable to NIST standards. The primary air is then supplied to a pipe nozzle having inner diameter of 8 mm, wall thickness of 1 mm and length of 500 mm. An orifice cap is fitted at the top end of the nozzle. The open end of the cap has inner diameter of 10 mm so that it is push fitted to the tube nozzle. The top surface has orifice hole. Five different orifice caps having orifice diameters of 0.5 mm, 1.0 mm, 1.5 mm, 2.0 mm and 2.5 mm (shown in Fig. 3) are used in the present work. The secondary air is metered through a venturi meter. The venturi is fabricated in-house with Aluminum rod. The venturi-meter has pipe diameter (D_p) of 5 mm and throat diameter (d_t) of 2.12 mm. The calibration is

performed with water for the entire range of flow Reynolds number investigated in the present study. A calibration curve is fitted between flow Reynolds number based on D_p and coefficient of discharge of venturi, C_d . During experiments, the pressure drop across venturi is measured with differential pressure transmitter (DPT) and line pressure with pressure gauge. The DPT is Furness Controls make and has range of 0 to 2kPa. Downstream of the venturi, flow control valve is installed to regulate the flow rate of the secondary air. The secondary air is then fed to isolation chamber. The isolation chamber having dimensions of 0.3 m x 0.3 m x 0.3 m is made of mild steel (MS). Two transparent glass windows are provided for visibility of the tube nozzle-orifice assembly and spacing. The chamber is made leak proof by use of rubber corks and gaskets at the tube and glass placing locations. A pressure tapping is provided to measure the cabin pressure. One end of the DPT is connected to the pressure tapping and other end kept open to ambient to measure the vacuum (suction pressure). The coaxial alignment of the orifice and the tube nozzle is done with the help of optical light beam. A scale is provided to measure the orifice exit to tube inlet distance. The spacing is adjusted by moving the top tube nozzle against a hole drilled in a gastight rubber cork. Smaller spacing is measured with Vernier scale. The isolation chamber is mounted on a stand for support.

The primary flow is first set with MFC to desired flow rate based on jet Reynolds number. The secondary flow control valve is kept in the close position. The vacuum pressure (ΔP) denoted by the DPT connected to the isolation chamber is noted. Then, the secondary line is set to some pressure (in the range of 0.5 to 2 bar). The flow control valve is slowly opened. The pressure inside the chamber will start increasing. The line pressure and pressure drop across the venturi (ΔP_v) are noted down for chamber pressure equal to ambient pressure.



1. Compressor, 2. Needle valve, 3. Pressure regulator with air filter, 4. Pressure gauge, 5. Differential pressure transmitter, 6. Venturi-meter, 7. Flow control valve, 8. Mass flow controller, 9. Tube nozzle, 10. Tube with orifice attached, 12. Isolation chamber with transparent window, 13. Scale.

Figure 1 Schematic of the experimental set up

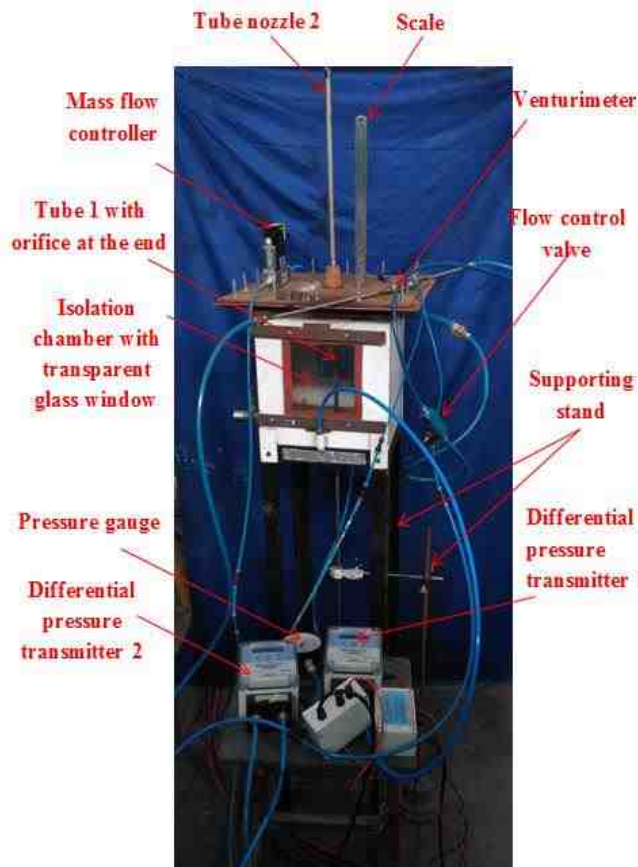


Figure 2 Photograph of the experimental set up

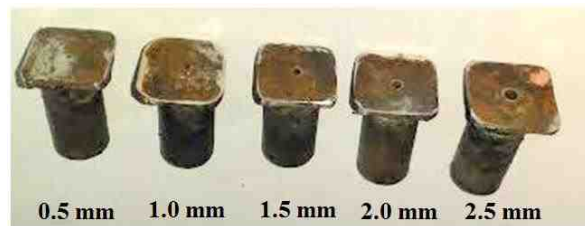


Figure 3 Photographs of orifice caps used in the present study

3.0 DATA REDUCTION

Jet Reynolds number is given by,

$$Re = \frac{\rho v d}{\mu} \quad (1)$$

Where, ρ is the of jet fluid in kg/m^3 and v is the jet exit velocity, d is the orifice diameter and μ is the viscosity of jet fluid.

$$\text{Entrainment coefficient, } e = \frac{\dot{m}_s}{\dot{m}_j} \quad (2)$$

Where, \dot{m}_s is the mass flow rate of secondary air in kg/s and \dot{m}_j is the mass flow rate of primary air through jet exit in kg/s .

$$\dot{m}_j = \frac{Re \pi d \mu}{4} \quad (3)$$

$$\dot{m}_s = \frac{\pi}{4} C_d d_t^2 \sqrt{\frac{2\rho\Delta P_v}{1-\beta^4}} \quad (4)$$

Where, C_d is the coefficient of discharge of venturi, d_t is throat diameter of venturi in m, β is the ratio of throat to pipe diameter, ΔP_v is the pressure drop across venturi in Pa and ρ is the density of secondary fluid at line pressure in kg/m³. The suction pressure created by closing the secondary flow to the isolation chamber is non-dimensionalised with the jet exit velocity. The pressure coefficient is defined as,

$$C_p = \frac{\Delta P}{\frac{1}{2}\rho v^2} \quad (5)$$

The Mach number is defined at the jet exit to judge the compressibility effects of the jet.

$$M = \frac{v}{c} \quad (6)$$

Where, c is the velocity in kg/s of sound in jet medium.

The uncertainty in experimental parameters is evaluated considering the uncertainties in measured parameters. The uncertainty in mass flow rate is 2 to 3%, pressure drop is 3 to 5%, Reynolds number is 2 to 5%, entrainment coefficient is 3 to 6%, pressure coefficient is 3 to 6% and Mach number is 2 to 4 %.

4.0 RESULTS AND DISCUSSION

The experiments are performed for varying jet flow rate, orifice diameters and spacing between orifice exit and tube inlet. The

entrainment ratio and the pressure coefficient are calculated from the flow rate and pressure measurements. The results are plotted as a function of non-dimensional orifice diameter (d/D), spacing between orifice and tube nozzle (Z/d) and jet Reynolds numbers (Re).

Figure 4 shows the distribution of entrainment coefficient (e) with non-dimensional spacing between orifice and pipe nozzle (Z/d) with variation in Reynolds number (Re) for normalized orifice diameter (d/D) of 0.15. It is observed from the graph that the entrainment coefficient shows a sharp rise with Z/d at the beginning stage and then reaches peak value at Z/d of 7 to 8. Further increase in spacing causes a gradual drop in the entrainment coefficient. The entrainment coefficient tends to zero for $Z/d > 100$. With the increase in jet Reynolds number, the peak value of entrainment coefficient rises slightly and the profile escalates. This is primarily due to the eddy formation and increased turbulence levels at higher Reynolds numbers. The location of peak entrainment is independent of jet Reynolds number. This depicts that the jet spread angle remains almost constant with the jet Reynolds number. Figure 5 shows the distribution of pressure coefficient (C_p) with non-dimensional spacing between orifice and pipe nozzle (Z/d) with variation in Reynolds number (Re) for normalized orifice diameter (d/D) of 0.1. It is observed that the pressure coefficient profile drops with the increase Reynolds number. The pressure being suction, the drop in C_p indicates higher potential for secondary air entrainment.

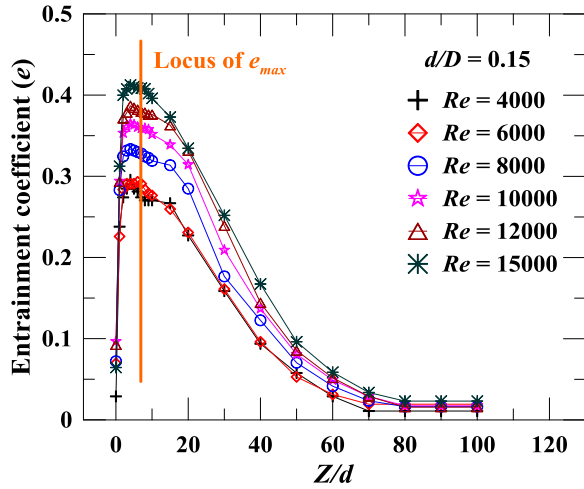


Figure 4 Distributions of entrainment coefficient (e) with Z/d for varied Re

Figure 6 shows the distribution of entrainment coefficient (e) with non-dimensional spacing between orifice and pipe nozzle (Z/d) with variation in normalized orifice diameter (d/D) for Reynolds number (Re) of 6000. It is seen from the plot that the peak entrainment coefficient for increasing d/D reduces due to the considerable reduction in eddy formation resulted from lower flow velocity. The profile flattens up for decrease in d/D making secondary air entrainment to a finite value at very large Z/d (~ 100). The locus of the peak entrainment coefficient shifts towards left for increased d/D . For a fixed D , with the increase in d , the spacing for which the jet width is equal to the tube nozzle diameter will decrease. The peak entrainment for d/D of 0.05 appears at Z/d of approximately 10. However, for d/D of 0.25, the peak entrainment occurs at Z/d of 2. The variation of pressure coefficient with Z/d for varied d/D is shown in Fig. 7. Considerable difference in pressure distributions is observed among all five orifices. At higher d/D , the drop of pressure is more rapid. However for, lower d/D s the distribution drops steadily.

Figure 8 shows the air entrainment for a cylindrical tube nozzle. The gas velocity gradually decreases as the jet ejects from the

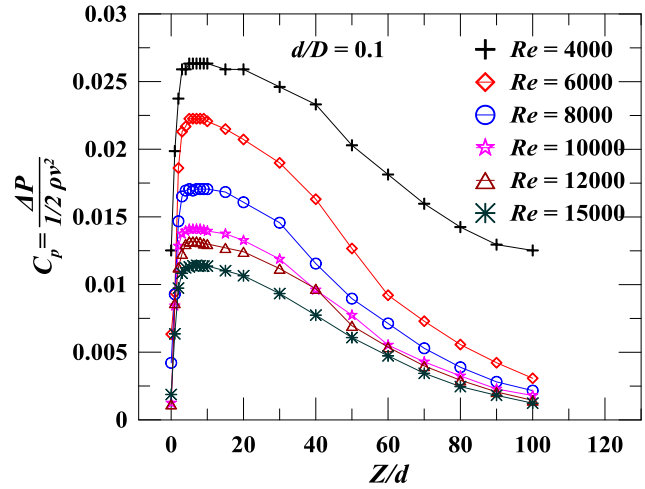


Figure 5 Distributions of pressure coefficient (C_p) with Z/d for varied Re

orifice due to the entrainment of secondary air from surrounding. The expansion region is characterised by rapid pressure build up inside the tube. The pressure gradually declines in the tube along the axis. At the exit, the pressure will be ambient and velocity will recover. If the jet width is exceeding the tube diameter at the entry location, the jet will split and only a part of it will propagate through the tube. The rest fluid will be accumulated inside the isolation chamber and gets recirculated and mixes with the secondary air and the pressure drop falls-off. Thus, the peak entrainment coefficient is obtained for the entry location of the tube such that the tube diameter is approximately equal to the tube diameter. For increased orifice diameter, the shift in location of the peak entrainment towards the orifice side is because of increased jet width.

The variation in peak entrainment coefficient (e_{max}) with Re and d/D is shown in Fig. 9. With the increase in Reynolds number, the peak entrainment coefficient also hikes. However, for increased d/D , the peak entrainment coefficient drops. The flow in case of $d/D = 0.05$ is almost compressible for all Reynolds numbers. Thus the jet gets expanded as it ejects and the entrainment coefficient drops. Figure 10 shows the jet exit

Mach number (M) with variation in Re for varied d/D . It is seen that the exit jet flow is under expanded for $d/D = 0.05$ for all

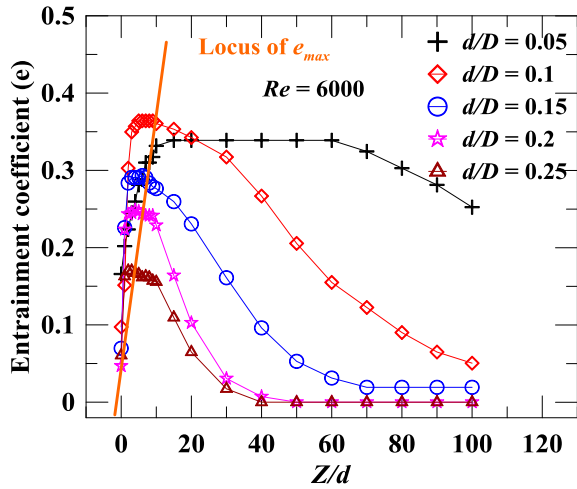


Figure 6 Distributions of entrainment coefficient (e) with Z/d for varied d/D

Reynolds numbers and for $d/D = 0.1$ for higher Reynolds numbers.

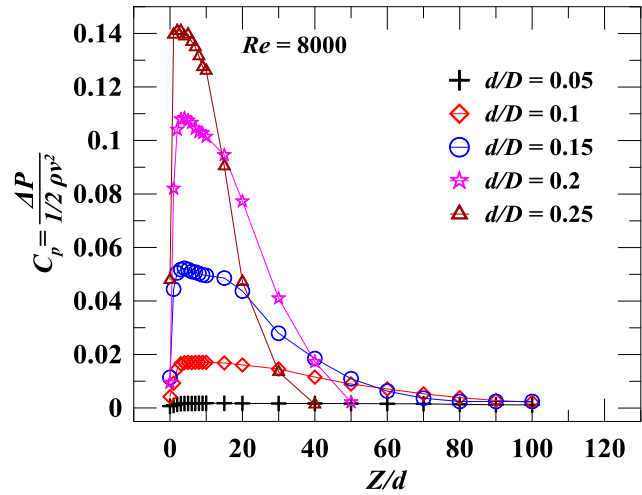


Figure 7 Distributions of pressure coefficient (C_p) with Z/d for varied d/D

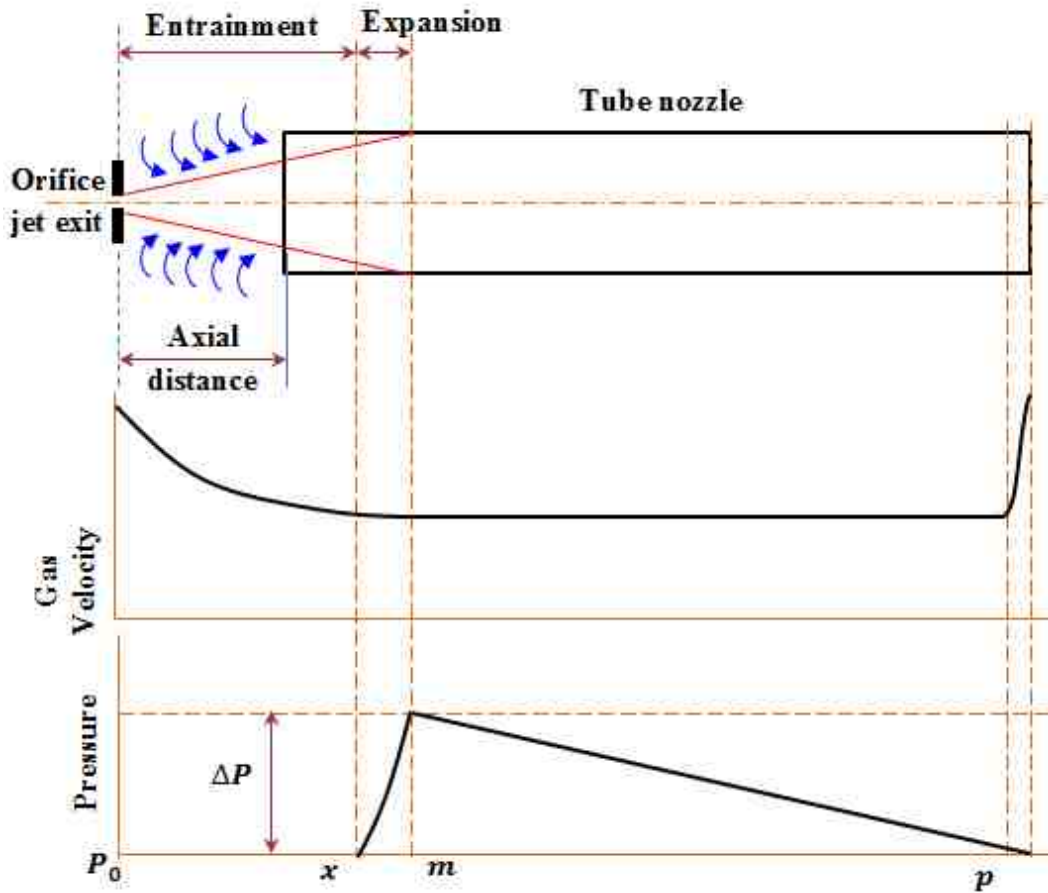


Figure 8 Air entrainment for a cylindrical tube nozzle [4]

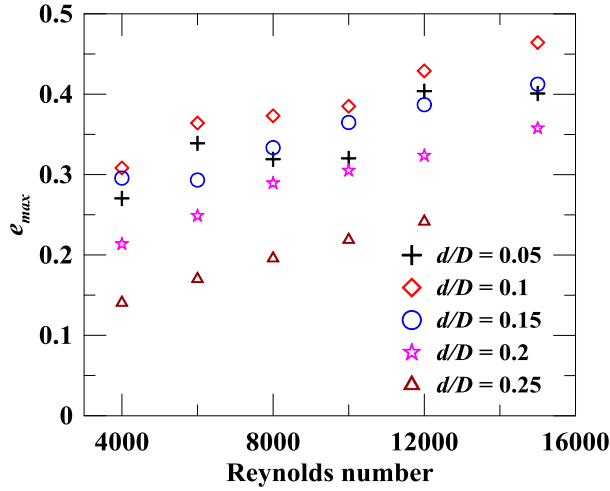


Figure 9 Peak entrainment coefficient (e_{max}) variation with Re for varied d/D

The peak entrainment coefficient is averaged ($(e_{max})_{avg}$) for fixed Re and fixed d/D and plotted respectively in Figures 11 and 12. The overall average of peak entrainment coefficient is 0.318 which is in well agreement with the value of 0.32 quoted by Ricou and Spalding [16].

The half-jet width of a turbulent jet at any axial location (Z) is given by [17],

$$R = \frac{1}{5} \left(Z + \frac{5d}{2} \right) \quad (7)$$

As the jet with approaches the tube diameter (D),

$$D = \frac{2}{5} \left(Z + \frac{5d}{2} \right) \quad (8)$$

On rearranging,

$$\frac{Z}{d} = \frac{5}{2} \left(\frac{D}{d} - 1 \right) \quad (9)$$

Figure 13 shows the plot of location of peak entrainment obtained experimentally and analytically. The experimental results match reasonably well with the experiments. The lower value of experimental Z/d indicates that the maximum entrainment occurs at the location where the jet width is slightly lower than the tube diameter.

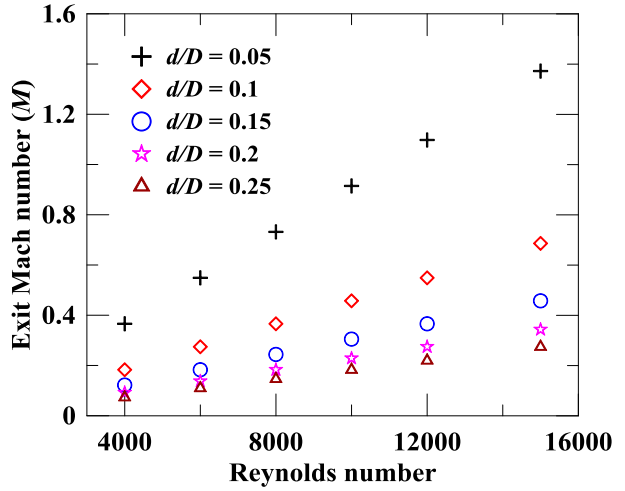


Figure 10 Exit Mach number (M) variation with Re for varied d/D

5.0 CONCLUSIONS

Jet entrainment has variety of engineering applications such as mixing tube of self-aspirating burners, pulse jet filter bags, synthetic jet cooling, gas turbine blade cooling etc. The entrainment plays favorable role in mixing of two gases and adverse role in thermal dilution of the jet. The present study attempted in experimental determination of the parameters associated with jet entrainment. The following are the major findings of the present study:

- Entrainment coefficient shows slight increment with Reynolds number
- The location of peak entrainment coefficient is independent of Reynolds number
- The pressure coefficient drops with the Reynolds number
- Increment in d/D causes dip in entrainment coefficient
- With the increase in d/D , the peak entrainment is observed at lower axial distances
- Pressure coefficient distribution amplifies and narrows with increase in d/D
- Overall entrainment coefficient of 0.318 is obtained

- Peak entrainment is obtained at the location where the jet width is comparable with the tube diameter

The present study contributes the entrainment data to the scientific community that can be utilised for practical applications.

NOMENCLATURE

c speed of sound, m/s
 C_d coefficient of discharge
 C_p pressure coefficient
 d orifice diameter, m
 D tube diameter, m
 D_p pipe diameter of venturi, m

d_t throat diameter of venturi, m
 e entrainment coefficient
 M Mach number
 \dot{m} mass flow rate, kg/s
 R half jet width, m
 Re Reynolds number
 v jet velocity, m/s
 Z axial distance, m
 ΔP vacuum pressure in isolation chamber, Pa
 ΔP_v pressure drop across the venturi, Pa

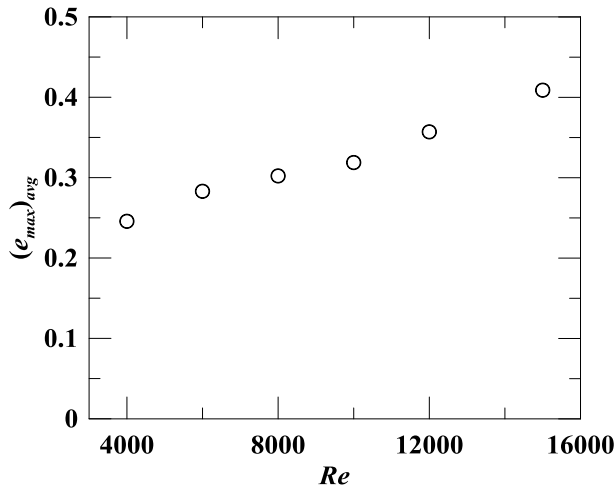


Figure 11 Average of peak entrainment coefficient (e_{max}) for all d/D with Re

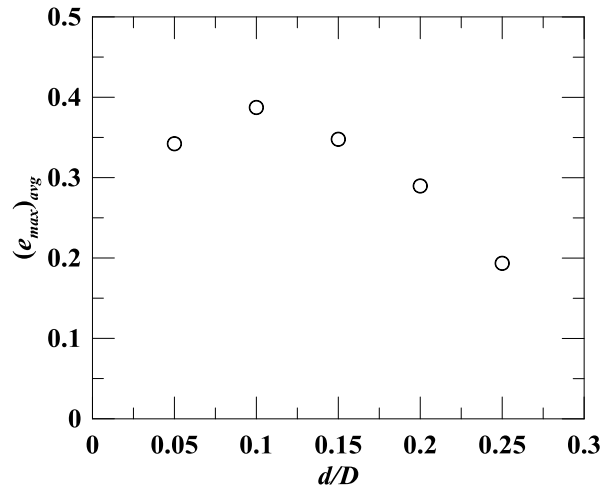


Fig. 12 Average of peak entrainment coefficient (e_{max}) for all Re with d/D

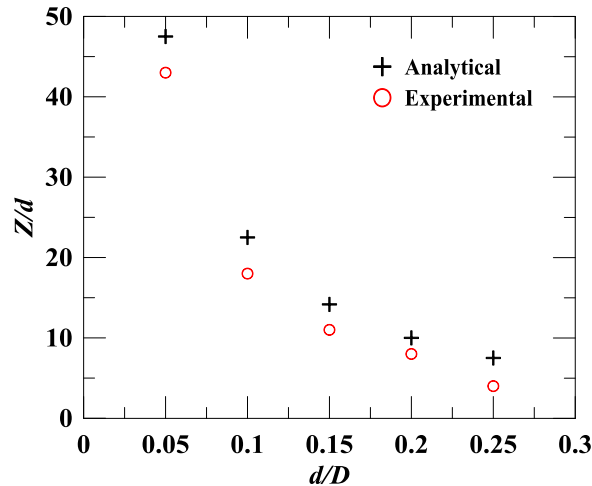


Figure 13 Stand-off distance for pipe nozzle from orifice for maximum entrainment

Greek letters

β ratio of throat to pipe diameter of venturi

μ viscosity, Pa.s

ρ density, kg/m³

Subscripts

avg average

j jet

max maximum

s secondary

Abbreviations

DPT Differential pressure transmitter

MFC mass flow controller

MS Mild steel

REFERENCES

- [1] Pavlova, A. and Amitay, M., 2006. Electronic cooling using synthetic jet impingement. *Journal of heat transfer*, 128(9), pp.897-907.
- [2] Han, J.C., Dutta, S. and Ekkad, S., 2012. *Gas turbine heat transfer and cooling technology*. CRC Press.
- [3] Han, B. and Goldstein, R.J., 2001. Jet-impingement heat transfer in gas turbine systems. *Annals of the New York Academy of Sciences*, 934(1), pp.147-161.
- [4] Morcos, V.H., 1994. Flame characteristics of liquefied petroleum gas with primary air entrainment for upright cylindrical burners. *Energy*, 19(4), pp.405-414.
- [5] Fulford, D., 1996. *Biogas stove design*. Reading, UK: Kingdom Bioenergy, Ltd.
- [6] Jones, H.R.N., 1989. *The application of combustion principles to domestic gas burner design*. Taylor & Francis.
- [7] Elbe, G.V. and Grumer, J., 1948. Air entrainment in gas burners. *Industrial & Engineering Chemistry*, 40(6), pp.1123-1129.
- [8] Fan, J., Eves, J., Thompson, H.M., Toropov, V.V., Kapur, N., Copley, D. and Mincher, A., 2011. Computational fluid dynamic analysis and design optimization of jet pumps. *Computers & Fluids*, 46(1), pp.212-217.
- [9] Dennis, R., Wilder, J.E. and Harmon, D.L., 1981. Predicting pressure loss for pulse jet filters. *Journal of the Air Pollution Control Association*, 31(9), pp.987-992.
- [10] Schildermans, I., Baeyens, J. and Smolders, K., 2004. Pulse jet cleaning of rigid filters: a literature review and introduction to process modelling. *Filtration & separation*, 41(5), pp.26-33.
- [11] Lu, H.C. and Tsai, C.J., 1999. Influence of design and operation parameters on bag-cleaning performance of pulse-jet baghouse. *Journal of Environmental Engineering*, 125(6), pp.583-591.
- [12] Rajaratnam, N., 1976. *Turbulent jets* (Vol. 5). Elsevier.
- [13] Namkhat, A. and Jugjai, S., 2010. Primary air entrainment characteristics for a self-aspirating burner: Model and experiments. *Energy*, 35(4), pp.1701-1708.
- [14] Yadav, H., Agrawal, A. and Srivastava, A., 2016. Mixing and entrainment characteristics of a pulse jet. *International Journal of Heat and Fluid Flow*, 61, pp.749-761.
- [15] MacGregor, S.A., 1991. Air entrainment in spray jets. *International journal of heat and fluid flow*, 12(3), pp.279-283.
- [16] Ricou, F.P. and Spalding, D.B., 1961. Measurements of entrainment by axisymmetrical turbulent jets. *Journal of fluid mechanics*, 11(1), pp.21-32.
- [17] Lee, J.H.W. and Chu, V., 2012. *Turbulent jets and plumes: a Lagrangian approach*. Springer Science & Business Media.

Presenting author Biodata

Name : Pramod Kuntikana

Designation : Research Scholar

Company : Indian Institute of Technology,
Bombay, Mumbai, India.

Qualification : Master of Technology (M-Tech)
Pursuing PhD.

Area of Expertise : Impinging flame jets, air jets, jet flow,
combustion

Significant Achievements: Graduate Research Award, IIT Bombay, 2016.



Number of Papers Published in Journals: Eight

Number of Papers Published in Conferences: Five